THE JOURNAL OF PHYSICAL CHEMISTRY LETTERS
A JOURNAL OF THE AMERICAN CHEMICAL SOCIETY

pubs.acs.org/JPCL

Letter

Anisotropic Carrier Mobility and Spectral Fingerprints of Two-Dimensional γ-Phosphorus Carbide with Antisite Defects

Konstantin P. Katin, Mikhail M. Maslov, Vladimir R. Nikitenko, Alexey I. Kochaev, Savas Kaya,* and Oleg V. Prezhdo*

Cite This: *J. Phys. Chem. Lett.* 2023, 14, 214–220

Read Online

ACCESS | Metrics & More | Article Recommendations | Supporting Information

ABSTRACT: We apply density functional theory to study carrier mobility in a γ-phosphorus carbide monolayer. Although previous calculations predicted high and anisotropic mobility in this material, we show that the mobility can be significantly influenced by common antisite defects. We demonstrate that at equilibrium concentrations defects do not inhibit carrier mobility up to temperatures of 1000 K. However, defects can change the mobility at high nonequilibrium concentrations of about 10^{-4} to 10^{-2} defects per atom. At the low end of this concentration range, defects act as traps for charge carriers and inhibit their mobility. At the high end of this range, defects change the effective carrier masses and deformation potentials, and they can lead to both an increase and a decrease in mobility. We also report the Raman and IR spectra associated with antisite defects. We predict new vibrational modes and shifts of the existing modes due to the defects.

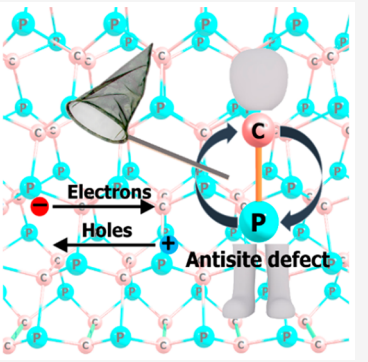

Graphene was the first synthesized two-dimensional (2D) material in which electrons and holes demonstrate exceptionally high carrier mobility. Theoretical estimates of the room-temperature electron and hole mobility in graphene are about 10^6 and 10^4 cm^2 V^{-1} s^{-1}, respectively.[1] However, measured mobility is restricted substantially by many factors, including grain boundaries,[2] influence of substrates,[3] adsorbed pollutants,[4] flexural phonons,[5] and point defects.[6] Moreover, high carrier mobility of graphene is associated with the linear dispersion relation near the Dirac cone. Therefore, high mobility is possible only in freestanding suspended monolayer. Opening of a band gap by different methods (interaction with substrate, mechanical strain, functionalization) leads to drastic reduction in mobility.[7] Therefore, electronic engineers are interested in alternative 2D materials, which combine moderate band gap with high carrier mobility.

Single layer black phosphorus, phosphorene, is an example of such a material.[8] Its band gap is much higher than that for bulk phosphorus and reaches 1.5 eV.[9] In addition, phosphorene is much less flexible compared to graphene, and therefore two-phonon scattering does not reduce carrier mobility in phosphorene at reasonable carrier concentrations of about 10^{13} cm^{-2}.[10] This is why phosphorene is a strong competitor to graphene as a basic material for nanoelectronic devices.[11] However, phosphorene has disadvantages compared to graphene, such as insufficient stability at ambient conditions[12] and low vacancy formation energy.[13]

2D phosphorus carbides (PC) are a new family of phosphorene-like materials, and some of them demonstrate advantages over both graphene and phosphorene. The first 2D PC was synthesized recently by exfoliation from 3D phosphorus carbide[14] and by the carbon doping technique.[15] Depending on the features of the structure and the ratio between carbon and phosphorus, 2D PC can exhibit metallic or semiconductor properties. Some of 2D PCs are wide-band gap semiconductors.[16] Another advantage of 2D PC is their high environmental stability.[17] Due to the mechanical strength of 2D PC, their electronic structures can be tuned by mechanical deformations.[18] In contrast to graphene, 2D PC are intrinsically biocompatible.[19]

Different structural forms of 2D PC are suitable for many applications. According to the *ab initio* calculations reported by Yu *et al.*,[20] the PC_6 allotrope demonstrates very high and anisotropic carrier mobility (about 2×10^5 cm^2 V^{-1} s^{-1}). In addition, it absorbs light in the 200−300 nm wavelengths range,[20] which is useful for photovoltaics. The α-phase of 2D PC provides directed migration of biomolecules along its surface.[21] The β-phase of 2D PC exhibits exceptional electrocatalityc activity to hydrogen evolution reaction.[22]

The presence of two chemical elements (carbon and phosphorus) implies appearance of antisite point defects (two neighboring atoms are swapped). According to our previous study,[23] the formation energy of such defect in 2D PC is 1.28 eV;

Received: October 31, 2022
Accepted: December 27, 2022
Published: December 30, 2022

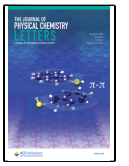

https://doi.org/10.1021/acs.jpclett.2c03297
J. Phys. Chem. Lett. 2023, 14, 214–220

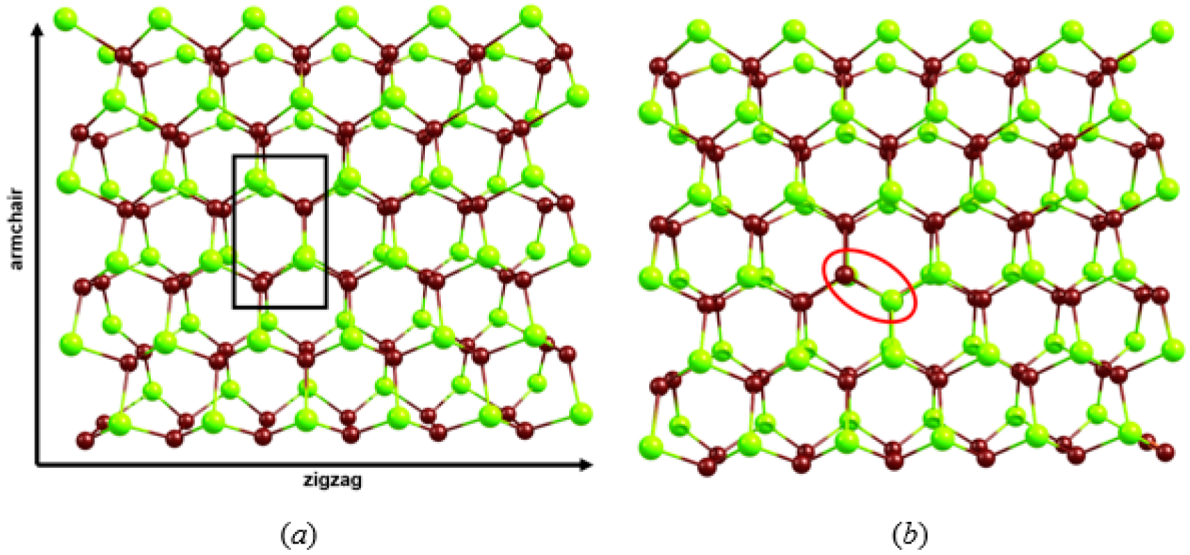

Figure 1. Pristine 2D γ-PC bilayer (a) and the same system with the antisite defect (b). Brown and green balls represent carbon and phosphorus atoms, respectively. The layers are covalently bonded via C−C interlayer bonds. The black rectangle in part a shows the primitive unit cell P_4C_4. The red ellipse in part b highlights the antisite defect.

Table 1. Calculated Charge Carrier Effective Masses (m_a* and m_z*, in Units of Electron Mass m_0), Mobility (μ_a and μ_z, cm^2 V^{-1} s^{-1}), Deformation Potentials (δ_a and δ_z, eV), and Relaxation Times (τ_a and τ_z, ps) in 2D γ-PC along the Armchair and Zigzag Directions at Different Defects Concentrations (Defects per Atom)[a]

conc	m_a*	m_z*	μ_a	μ_z	δ_a	δ_z	τ_a	τ_z
				electrons				
1/64	$0.48m_0$	$0.58m_0$	6.21×10^5	6.83×10^5	−0.19	−0.16	169.8	225.5
1/144	$0.48m_0$	$0.53m_0$	2.90×10^6	1.39×10^6	0.09	0.12	791.7	419.4
1/256	$0.47m_0$	$0.49m_0$	2.80×10^5	8.75×10^4	0.30	0.51	74.9	24.4
0	$0.47m_0$	$0.46m_0$	2.39×10^5	8.27×10^4	0.33	0.55	63.9	21.7
				holes				
1/64	$1.57m_0$	$1.75m_0$	7.73×10^2	1.19×10^2	−1.68	−3.94	0.69	0.12
1/144	$1.32m_0$	$1.51m_0$	7.40×10^2	1.93×10^2	−2.03	−3.61	0.56	0.17
1/256	$0.98m_0$	$1.06m_0$	1.14×10^3	5.22×10^2	−2.23	−3.08	0.64	0.32
0	$0.63m_0$	$0.66m_0$	1.66×10^3	1.51×10^3	−2.90	−2.89	0.60	0.57

[a] T = 300 K. Results for defect-free 2D γ-PC are presented for comparison.

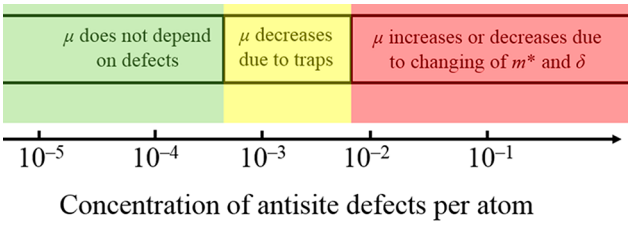

Figure 2. Mechanisms of the influence of antisite defects on charge carrier mobility μ in 2D γ-PC at different defects concentrations.

much lower than those of others defects. In addition, antisite defects are thermally stable.[23] Therefore, they can appear at high temperatures, which are necessary for fabrication or processing of nanodevices.

Here, we investigate carrier mobility as a function of the antisite defects concentration. We focus on the γ-phase of PC (γ-PC), which is a representative example of the 2D PC material suitable for nanoelectronics. This phase is of interest because it combines a wide band gap (2.65 eV) with ultrahigh conductivity and excellent structural stability.[24] Based on the *ab initio* approach, we estimate carrier mobility in the defected sheet for a broad range of defect concentrations. We also simulate the infrared and Raman fingerprints of the defected γ-PC to facilitate spectroscopic identification of the antisite defects.

The mobility of electrons and holes in the armchair and zigzag directions are calculated from their effective masses and the corresponding deformation potential constant. Such approach proved its validity and accuracy for estimation of mobility in similar systems, phosphorene and 2D CP_6.[20] Mobility μ was defined as

$$\mu_i = e\hbar^3 E_i/(k_B T m_i^* m^* \delta_i^2) \quad (1)$$

Here e, $\hbar$, and k_B are elementary charge, and Planck's and Boltzmann's constants, respectively; E_i, m_i*, and δ_i are 2D Young modulus, effective carrier mass and deformation potential constant in the corresponding direction i; i = "a" or "z" for the armchair or zigzag directions; m* is the mean effective carrier mass estimated as $m^* = \sqrt{m_a^* m_z^*}$; and T is temperature.

The two-dimensional Young modulus E_i is calculated as[25]

$$E_i = (\partial^2 U/\partial \varepsilon_i^2)/S \quad (2)$$

In this formula, $S = a_a a_z$ is the area of the considered cell with lattice vectors a_a and a_z, $\varepsilon_i = \Delta a_i/a_i$ is the cell deformation along the "a" or "z" direction due to elongation of the corresponding

https://doi.org/10.1021/acs.jpclett.2c03297
J. Phys. Chem. Lett. 2023, 14, 214−220

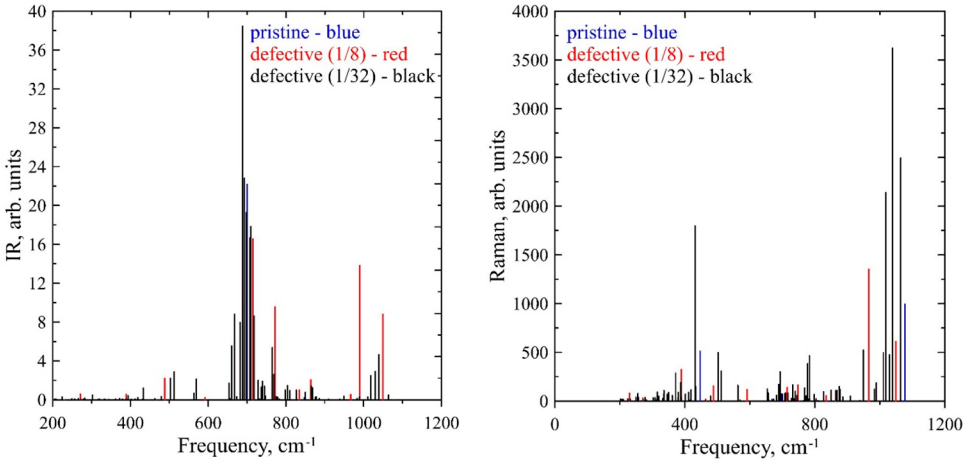

Figure 3. Calculated infrared (a) and Raman (b) spectra of pristine and two defective 2D γ-PC bilayers at concentrations of 1/8 and 1/32 defects per atom.

lattice vector a_i, U is the total energy of the deformed cell. To calculate the second derivative numerically, we compute the values of U at deformations of 0, 1, and 2% in each of the two directions.

The effective masses of electrons/holes are calculated as

$$m_i^* = \hbar^2/(\partial^2 E/\partial k_i^2) \quad (3)$$

Here, E is the energy of the valence or conductance band for holes or electrons, respectively; the second derivative is taken at the maximum of the valence band or minimum of the conductance band; k_i is projection of the wavenumber on the armchair (i = "a") or zigzag (i = "z") direction.

The deformation potential constant δ_i is defined as

$$\delta_i = \Delta E/\varepsilon_i \quad (4)$$

Here, ΔE is the change of the valence band maximum (for holes) or the conduction band minimum (for electron) due to the applied mechanical deformation ε_i. The carrier relaxation times τ_i are calculated as

$$\tau_i = \mu_i m_i^*/e \quad (5)$$

γ-PC has an orthorhombic two-dimensional lattice, and its primitive rectangular unit cell P_4C_4 contains 8 atoms,[23] as shown in Figure 1a. The armchair and zigzag directions along two perpendicular lattice vectors are further labeled as "a" and "z", respectively. For pristine γ-PC, we consider 1×2 and 2×4 near-square unit cells, containing 16 and 64 atoms, respectively. Defective γ-PC cells are obtained via swapping of the neighboring carbon and phosphorus atoms located in the same layer, see Figure 1b. We consider 2×4, 3×6 and 4×8 almost square unit cells, each having a single antisite defect. Therefore, the defect concentration, defined by the atom ratio, are 1/64, 1/144 and 1/256, respectively. I.e., there is 1 defect per 256 atoms in the 4×8 simulation cell.

2D Young moduli E_a and E_z, calculated for pristine 2D γ-PC, are equal to 265 and 252 Pa, respectively. Consideration of unit cells of different sizes ranging from 2×4 to 4×8 leads to a variation of these values of less than 1 Pa. Since the concentration of defects in a real material is quite low, we adopted the same values when calculating mobility in defective bilayers according to the formula 1. Effective masses, mobility, deformation potentials and relaxation times for both electrons and holes at different defect concentrations are listed in Table 1. The carrier mobility in 2D γ-PC is moderately anisotropic. Defects at the lowest considered concentration (1/256 defects per atom) slightly change the effective masses and deformation potentials compared to the defect-free material. However, higher defects concentrations, which are possible under normal conditions, result in significant reorganization of the band structure and even change in the sign of the deformation potential. In particular, at a certain concentration, the deformation potential turns to zero, which leads to unrealistically high mobility estimates according to formula 1.

However, realistic defect concentrations in thermal equilibrium are much smaller than the minimal value presented in Table 1. At low concentrations, defects do not influence the effective masses and deformation potentials included in the formula 1. However, they can still limit the carrier mobility substantially. At low concentrations, new localized states of charge carriers associated with defects appear inside the band gap. The partial density of electronic states proving the association of the in-gap states with the defect is shown in Figure S1. The probability of tunnel jumps between these states is negligible due to large distances between defects. Therefore, defects-associated states act as traps for the charge carriers.

It should be noted that eqs 1−4 determine trap-free mobility. Mobility μ_{ti} controlled by traps with energy depth Δ can be estimated from the multiple trapping and release model[26,27] as

$$\mu_{ti} = \mu_i \Big/ \left(1 + \frac{n_t}{n_c} \exp(\Delta/k_B T)\right) \quad (6)$$

Here, n_t is the surface density of defects (traps), and n_c is the effective surface density of conductive states for charge carriers (electrons in the conductance band or holes in the valence band). In the 2D system considered here, the density of states near the band edge is $m^*/(\pi\hbar^2)$. Therefore, one can estimate the effective surface density of conductive states as

$$n_c = m^* k_B T/(\pi\hbar^2) \quad (7)$$

According to formulas 6 and 7, defects substantially decrease the mobility of charge carriers, when their concentration exceeds

https://doi.org/10.1021/acs.jpclett.2c03297
J. Phys. Chem. Lett. 2023, 14, 214−220

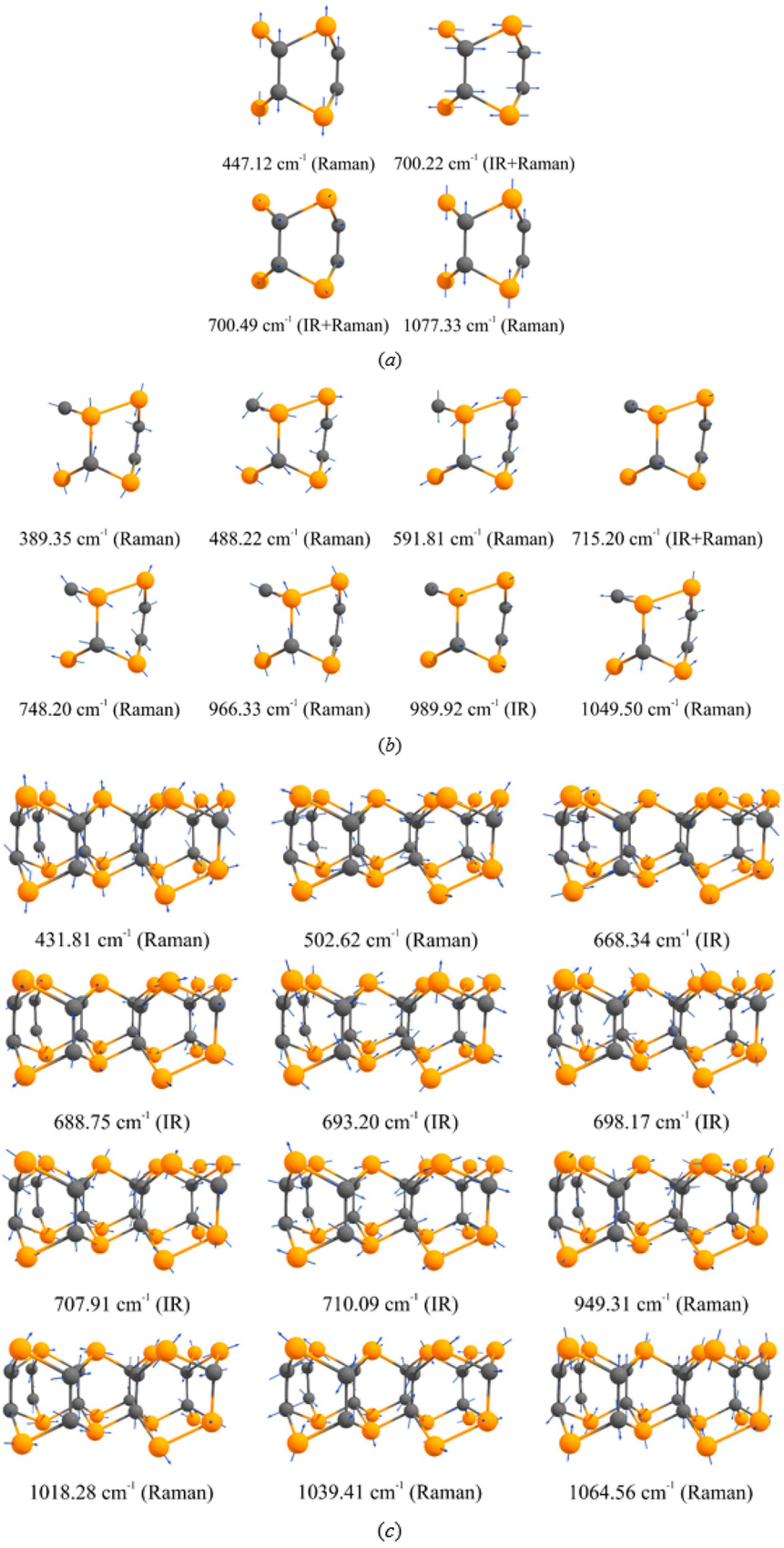

Figure 4. Most active infrared and Raman vibrational modes of the pristine (a) and two defective 2D γ-PC bilayers at concentrations of 1/8 (b) and 1/32 (c) defects per atom, respectively.

https://doi.org/10.1021/acs.jpclett.2c03297
J. Phys. Chem. Lett. 2023, 14, 214−220

the critical value n_{t0}, which is defined by the following expression:

$$n_{t0} = \frac{m^* k_B T}{\pi \hbar^2} \exp(-\Delta / k_B T) \quad (8)$$

The value of Δ for the antisite defect in 2D γ-PC is equal to 0.4 eV for both electrons and holes.[23] According to eq 8, at room temperature the critical densities of defects are 4.6×10^{16} m^{-2} and 6.3×10^{16} m^{-2} for electrons and holes, respectively (taking the minimum of m_a* and m_z* from the Table 1 as m*). The equilibrium surface density of the most probable antisite defects n_{eq} at temperature T can be estimated as

$$n_{eq} = n_{eq0} \exp(-E_f / k_B T) \quad (9)$$

Here, E_f = 1.28 eV is the formation energy of the antisite defect, and $n_{eq0} = 2.4 \times 10^{19}$ m^{-2} is the prefactor, which is equal to the surface density of atoms in perfect γ-PC.[23] Calculations show that $n_{eq} \ll n_{t0}$ throughout a reasonable temperature range, $T <$ 1000 K. However, the estimated comparably low thermodynamic probability of point defect formation in 2D γ-PC can be much higher during its manufacturing. Note that high density of defects is common for most 2D materials, since their synthesis can be governed by kinetic factors.[23] Furthermore, the defect concentration in γ-PC can be controlled by means of defect engineering.[28] Figure 2 summarizes different mechanisms of the influence of antisite defects on charge carrier mobility.

Spectroscopic technique is a useful tool for independent observation of antisite defects that limit carrier mobility in 2D γ-PC. Figure 3 shows spectral fingerprints of defective 2D γ-PC calculated at concentrations of 1/8 and 1/32 defects per atom, in comparison with the defects-free system. Such high concentrations are used to highlight the features of the spectra near the defect site. The most active oscillation frequencies are shown in detail in Figure 4. Significant defects-induced shifts of active frequencies prove that defects can be clearly detected by spectroscopic methods. It is not surprising that the defect leads to the appearance of new active frequencies due to strain of the existing bonds near the defect and formation of new types of bonds. In addition, the vibrations of defective systems are less selective with respect to the polarization of incident radiation. As can be seen from Figure 4, vibrations of the newly formed PC interlayer bonds are observed at the frequencies of 966 and 949 cm^{-1} for 1/8 and 1/32 defects per atom, respectively. The latter frequency is closer to the value that would be observed at an experimentally relevant defect concentration. Note the significant red shift of both the highest and the lowest Raman frequencies associated with out-of-plane vibrations. In addition, the defects lead to the splitting of the well-defined infrared peak at 700 cm^{-1} into a variety of peaks in the 660−980 cm^{-1} range.

High carrier mobility is a feature of many 2D materials, including graphene and phosphorus carbides. This feature makes these materials attractive for electronics applications. However, the mobility in real materials may be limited by defects. This limitation can determine the resistance of electronics devices to temperature, radiation, and other environmental factors. In this paper, through the first-principle calculations we have considered two possible mechanisms of the influence of defects on the charge carrier mobility in 2D γ-PC, and identified spectral fingerprints of the defects. The determined stability range of this material is quite wide, confirming usefulness of 2D γ-PC and similar 2D modifications of phosphorus carbide as the elemental basis for novel electronics.

COMPUTATIONAL DETAILS

Density functional theory calculations were performed with the Perdew−Burke−Ernzerhof (PBE) exchange-correlation functional and projector-augmented wave pseudopotentials[29,30] with the kinetic energy cutoff for wave functions and charge density of 100 and 600 Ry, respectively. A Monkhorst−Pack 12 × 12 × 1 k-point grid[31] was used. The first-order Methfessel−Paxton scheme[32] with a smearing of 0.02 Ry was applied as it is implemented in the Quantum Espresso package.[33,34] For equilibrium sheets, the lattice vectors were optimized along with atomic coordinates, whereas for stretching sheets the vectors were kept unchanged to provide desired deformation. The out-of-plane periodic vector was equal to 30 Å for all systems to exclude any interaction with periodic images. Grimme's D3 dispersion corrections[35] were introduced for accurate description of possible noncovalent interaction in the considered 2D bilayer systems. Calculations of the phonon frequencies as well as Raman and IR spectra were performed with the density functional perturbation theory (DFPT) method[36] combined with the Perdew−Wang (PW91) exchange-correlation functional[37] and the Troullier−Martins norm-conserving pseudopotentials.[38] Geometries of all considered systems were reoptimized before calculations of the vibrational modes. For all DFTP calculations, the cutoff energies for wave functions and charge densities were 300 and 1200 Ry, respectively. To make sure of the reliability of the results obtained, we also considered a 3 × 4 cell with two defects per cell. Three different relative locations of the defect pairs were selected; see Figure S2. The corresponding bands structures are shown in the same figure, Figure S2. These data confirm that the location of defects has insignificant effect on the sheet band structure.

ASSOCIATED CONTENT

Supporting Information

The Supporting Information is available free of charge at https://pubs.acs.org/doi/10.1021/acs.jpclett.2c03297.

Simulation cell and partial density of states for 2D γ-PC with a single antisite defec and three configurations with two antisite defects and corresponding band structures (PDF)

AUTHOR INFORMATION

Corresponding Authors

Oleg V. Prezhdo − *Department of Chemistry, University of Southern California, Los Angeles 90089 California, United States;* orcid.org/0000-0002-5140-7500; Email: prezhdo@usc.edu

Savas Kaya − *Health Services Vocational School, Department of Pharmacy, Sivas Cumhuriyet University, Sivas 58140, Turkey;* orcid.org/0000-0002-0765-9751; Email: savaskaya@cumhuriyet.edu.tr

Authors

Konstantin P. Katin − *Department of Condensed Matter Physics, National Research Nuclear University "MEPhI", Moscow 115409, Russian Federation;* orcid.org/0000-0003-0225-5712

https://doi.org/10.1021/acs.jpclett.2c03297
J. Phys. Chem. Lett. 2023, 14, 214−220

Mikhail M. Maslov − *Department of Condensed Matter Physics, National Research Nuclear University "MEPhI", Moscow 115409, Russian Federation;* orcid.org/0000-0001-8498-4817

Vladimir R. Nikitenko − *Department of Condensed Matter Physics, National Research Nuclear University "MEPhI", Moscow 115409, Russian Federation;* orcid.org/0000-0001-8673-5048

Alexey I. Kochaev − *Research and Education Center "Silicon and Carbon Nanotechnologies", Ulyanovsk State University, Ulyanovsk 432017, Russian Federation;* orcid.org/0000-0002-3521-5891

Complete contact information is available at: https://pubs.acs.org/10.1021/acs.jpclett.2c03297

Notes

The authors declare no competing financial interest.

■ ACKNOWLEDGMENTS

V.R.N. acknowledges support of the Russian Science Foundation, Project 22-22-00612. O.V.P. acknowledges support of the US Department of Energy, Project DE-SC0014429.

■ REFERENCES

(1) Long, M.-Q.; Tang, L.; Wang, D.; Wang, L.; Shuai, Z. Theoretical Predictions of Size-Dependent Carrier Mobility and Polarity in Graphene. *J. Am. Chem. Soc.* **2009**, *131*, 17728−17729.

(2) Song, H. S.; Li, S. L.; Miyazaki, H.; Sato, S.; Hayashi, K.; Yamada, A.; Yokoyama, N.; Tsukagoshi, K. Origin of the Relatively Low Transport Mobility of Graphene Grown through Chemical Vapor Deposition. *Sci. Rep.* **2012**, *2*, 337.

(3) Scarfe, S.; Cui, W.; Luican-Mayer, A.; Ménard, J.-M. Systematic THz Study of the Substrate Effect in Limiting the Mobility of Graphene. *Sci. Rep.* **2021**, *11*, 8729.

(4) Chen, L.; Wang, L.; Shuai, Z.; Beljonne, D. Energy Level Alignment and Charge Carrier Mobility in Noncovalently Functionalized Graphene. *J. Phys. Chem. Lett.* **2013**, *4*, 2158−2165.

(5) Castro, E. V.; Ochoa, H.; Katsnelson, M. I.; Gorbachev, R. V.; Elias, D. C.; Novoselov, K. S.; Geim, A. K.; Guinea, F. Limits on Charge Carrier Mobility in Suspended Graphene Due to Flexural Phonons. *Phys. Rev. Lett.* **2010**, *105*, 266601.

(6) Ni, Z. H.; Ponomarenko, L. A.; Nair, R. R.; Yang, R.; Anissimova, S.; Grigorieva, I. V.; Schedin, F.; Blake, P.; Shen, Z. X.; Hill, E. H.; et al. On Resonant Scatterers as a Factor Limiting Carrier Mobility in Graphene. *Nano Lett.* **2010**, *10*, 3868−3872.

(7) Mir, S. H.; Yadav, V. K.; Singh, J. K. Recent Advances in the Carrier Mobility of Two-Dimensional Materials: A Theoretical Perspective. *ACS Omega* **2020**, *5*, 14203−14211.

(8) Liu, H.; Neal, A. T.; Zhu, Z.; Luo, Z.; Xu, X.; Tománek, D.; Ye, P. D. Phosphorene: An Unexplored 2D Semiconductor with a High Hole Mobility. *ACS Nano* **2014**, *8*, 4033−4041.

(9) Cai, Y.; Zhang, G.; Zhang, Y.-W. Layer-Dependent Band Alignment and Work Function of Few-Layer Phosphorene. *Sci. Rep.* **2015**, *4*, 6677.

(10) Rudenko, A. N.; Brener, S.; Katsnelson, M. I. Intrinsic Charge Carrier Mobility in Single-Layer Black Phosphorus. *Phys. Rev. Lett.* **2016**, *116*, 246401.

(11) Li, L.; Yu, Y.; Ye, G. J.; Ge, Q.; Ou, X.; Wu, H.; Feng, D.; Chen, X. H.; Zhang, Y. Black Phosphorus Field-Effect Transistors. *Nat. Nanotechnol.* **2014**, *9*, 372−377.

(12) Kim, J.-S.; Liu, Y.; Zhu, W.; Kim, S.; Wu, D.; Tao, L.; Dodabalapur, A.; Lai, K.; Akinwande, D. Toward Air-Stable Multilayer Phosphorene Thin-Films and Transistors. *Sci. Rep.* **2015**, *5*, 08989.

(13) Hu, W.; Yang, J. Defects in Phosphorene. *J. Phys. Chem. C* **2015**, *119*, 20474−20480.

(14) Huang, X.; Cai, Y.; Feng, X.; Tan, W. C.; Hasan, D. M. N.; Chen, L.; Chen, N.; Wang, L.; Huang, L.; Duffin, T. J.; et al. Black Phosphorus Carbide as a Tunable Anisotropic Plasmonic Metasurface. *ACS Photonics* **2018**, *5*, 3116−3123.

(15) Tan, W. C.; Cai, Y.; Ng, R. J.; Huang, L.; Feng, X.; Zhang, G.; Zhang, Y.-W.; Nijhuis, C. A.; Liu, X.; Ang, K.-W. Few-Layer Black Phosphorus Carbide Field-Effect Transistor via Carbon Doping. *Adv. Mater.* **2017**, *29*, 1700503.

(16) Guan, J.; Liu, D.; Zhu, Z.; Tománek, D. Two-Dimensional Phosphorus Carbide: Competition between sp^2 and sp^3 Bonding. *Nano Lett.* **2016**, *16*, 3247−3252.

(17) Kistanov, A. A.; Korznikova, E. A.; Huttula, M.; Cao, W. The Interaction of Two-Dimensional α- and β-Phosphorus Carbide with Environmental Molecules: A DFT Study. *Phys. Chem. Chem. Phys.* **2020**, *22*, 11307−11313.

(18) Shcherbinin, S. A.; Zhou, K.; Dmitriev, S. V.; Korznikova, E. A.; Davletshin, A. R.; Kistanov, A. A. Two-Dimensional Black Phosphorus Carbide: Rippling and Formation of Nanotubes. *J. Phys. Chem. C* **2020**, *124*, 10235−10243.

(19) Liu, Y.; Yang, Y.; Qu, Y.; Li, Y.-Q.; Zhao, M.; Li, W. Mild Lipid Extraction and Anisotropic Cell Membrane Penetration of α-Phase Phosphorene Carbide Nanoribbons by Molecular Dynamics Simulation Studies. *Phys. Chem. Chem. Phys.* **2020**, *22*, 23268−23275.

(20) Yu, T.; Zhao, Z.; Sun, Y.; Bergara, A.; Lin, J.; Zhang, S.; Xu, H.; Zhang, L.; Yang, G.; Liu, Y. Two-Dimensional PC6 with Direct Band Gap and Anisotropic Carrier Mobility. *J. Am. Chem. Soc.* **2019**, *141*, 1599−1605.

(21) Liu, Y.; Song, X.; Yang, Y.; Li, Y.-Q.; Zhao, M.; Mu, Y.; Li, W. Anisotropic Protein Diffusion on Nanosurface. *Nanoscale* **2020**, *12*, 5209−5216.

(22) Liang, X.; Wu, C.-M. L. Metal-Free Two-Dimensional Phosphorus Carbide as an Efficient Electrocatalyst for Hydrogen Evolution Reaction Comparable to Platinum. *Nano Energy* **2020**, *71*, 104603.

(23) Kistanov, A. A.; Nikitenko, V. R.; Prezhdo, O. V. Point Defects in Two-Dimensional γ-Phosphorus Carbide. *J. Phys. Chem. Lett.* **2021**, *12*, 620−626.

(24) Zhang, W.; Yin, J.; Zhang, P.; Tang, X.; Ding, Y. Two-Dimensional Phosphorus Carbide as a Promising Anode Material for Lithium-Ion Batteries. *J. Mater. Chem. A* **2018**, *6*, 12029−12037.

(25) Kochaev, A. Elastic Properties of Noncarbon Nanotubes as Compared to Carbon Nanotubes. *Phys. Rev. B* **2017**, *96*, 155428.

(26) Rose, A. An Outline of Some Photoconductive Processes. *RCA Rev.* **1951**, *12*, 362−414.

(27) Fowler, J. F. X-Ray Induced Conductivity in Insulating Materials. *Proc. R. Soc. A* **1956**, *236*, 464−480.

(28) Hu, Z.; Wu, Z.; Han, C.; He, J.; Ni, Z.; Chen, W. Two-Dimensional Transition Metal Dichalcogenides: Interface and Defect Engineering. *Chem. Soc. Rev.* **2018**, *47*, 3100−3128.

(29) Blöchl, P. E. Projector Augmented-Wave Method. *Phys. Rev. B* **1994**, *50*, 17953−17979.

(30) Kresse, G.; Joubert, D. From Ultrasoft Pseudopotentials to the Projector Augmented-Wave Method. *Phys. Rev. B* **1999**, *59*, 1758−1775.

(31) Monkhorst, H. J.; Pack, J. D. Special Points for Brillouin-Zone Integrations. *Phys. Rev.* **1976**, *13*, 5188−5192.

(32) Methfessel, M.; Paxton, A. T. High-Precision Sampling for Brillouin-Zone Integration in Metals. *Phys. Rev. B* **1989**, *40*, 3616−3621.

(33) Giannozzi, P.; Baroni, S.; Bonini, N.; Calandra, M.; Car, R.; Cavazzoni, C.; Ceresoli, D.; Chiarotti, G. L.; Cococcioni, M.; Dabo, I.; et al. QUANTUM ESPRESSO: A Modular and Open-Source Software Project for Quantum Simulations of Materials. *J. Phys. Cond. Matter* **2009**, *21*, 395502.

(34) Giannozzi, P.; Andreussi, O.; Brumme, T.; Bunau, O.; Buongiorno Nardelli, M.; Calandra, M.; Car, R.; Cavazzoni, C.; Ceresoli, D.; Cococcioni, M.; et al. Advanced Capabilities for Materials Modelling with Quantum ESPRESSO. *J. Phys. Cond. Matter* **2017**, *29*, 465901.

(35) Grimme, S.; Antony, J.; Ehrlich, S.; Krieg, H. A Consistent and Accurate Ab Initio Parametrization of Density Functional Dispersion Correction (DFT-D) for the 94 Elements H-Pu. *J. Chem. Phys.* **2010**, *132*, 154104.
(36) Baroni, S.; de Gironcoli, S.; Dal Corso, A.; Giannozzi, P. Phonons and Related Crystal Properties from Density-Functional Perturbation Theory. *Rev. Modern Phys.* **2001**, *73*, 515−562.
(37) Perdew, J. P.; Wang, Y. Accurate and Simple Analytic Representation of the Electron-Gas Correlation Energy. *Phys. Rev. B* **1992**, *45*, 13244−13249.
(38) Troullier, N.; Martins, J. L. Efficient Pseudopotentials for Plane-Wave Calculations. *Phys. Rev. B* **1991**, *43*, 1993−2006.

https://doi.org/10.1021/acs.jpclett.2c03297
J. Phys. Chem. Lett. 2023, 14, 214−220